Catalytic Formation of Cyclic Carbonates using Gallium Aminotrisphenolate Compounds and Comparison to their Aluminium Congeners: A Combined Experimental and Computational Study

ÁLVAREZ-MIGUEL, Lucía, BURGOA, Jesús Damián, MOSQUERA, Marta E. G., HAMILTON, Alex <http://orcid.org/0000-0001-7632-1319> and WHITEOAK, Christopher J.

Catalytic Formation of Cyclic Carbonates using Gallium Aminotrisphenolate Compounds and Comparison to their Aluminium Congeners: A Combined Experimental and Computational Study

Lucía Álvarez-Miguel,[a] Jesús Damián Burgoa,[a] Marta E. G. Mosquera,*[a] Alex Hamilton,*[b] and Christopher J. Whiteoak*[a]

This work reports on the use of gallium aminotrisphenolate compounds as catalysts for the synthesis of cyclic carbonates from epoxides and CO_2. The results show that they are highly active, and more so than the corresponding aluminium congeners. The catalyst system is applicable at low and elevated temperatures across a wide substrate scope including terminal, internal, multiple and fully deuterated epoxides. Applying low catalyst loadings has allowed for a TON of 344,000 to be obtained, highlighting their stability. A DFT investigation has confirmed that the gallium catalysts have lower energetic profiles compared to the aluminium congeners. Measurement of the Lewis acidity of both the gallium and aluminium aminotrisphenolate compounds using the Gutmann-Beckett method provides the experimental proof that the gallium compounds are more Lewis acidic than their aluminium congeners. Finally, Ab-Initio Molecular Dynamic (AIMD) simulations have investigated and quantified the dynamic behaviour of the catalytic systems, highlighting an important increase in fluxionality in some cases which helps to explain the increase in catalytic activity.

Introduction

The use of carbon dioxide (CO_2) as a cheap and readily available C1 source in fine and bulk chemical production is attracting significant interest from the scientific community. Indeed, many different applications of CO_2 as feedstock have been, and continue to be developed, usually based on catalytic approaches due to the high stability of the CO_2 molecule.[1] In this context, the atom efficient synthesis of cyclic carbonates from ring-strained epoxides (high energy substrates) and CO_2 (Scheme 1a) has attracted plenty of attention, primarily as a result of their well-established application as electrolytes in Li-ion batteries[2] and their utility as both monomers for polycarbonate synthesis[3] and non-isocyanate polyurethanes[4] or as synthetic intermediates.[5] Whilst a plethora of both heterogeneous[6] and homogenous catalysts[7] have been developed for this reaction over the last decade, catalysts that are truly "highly active" still remain relatively elusive. Successful homogeneous catalysts are often based on the activation of

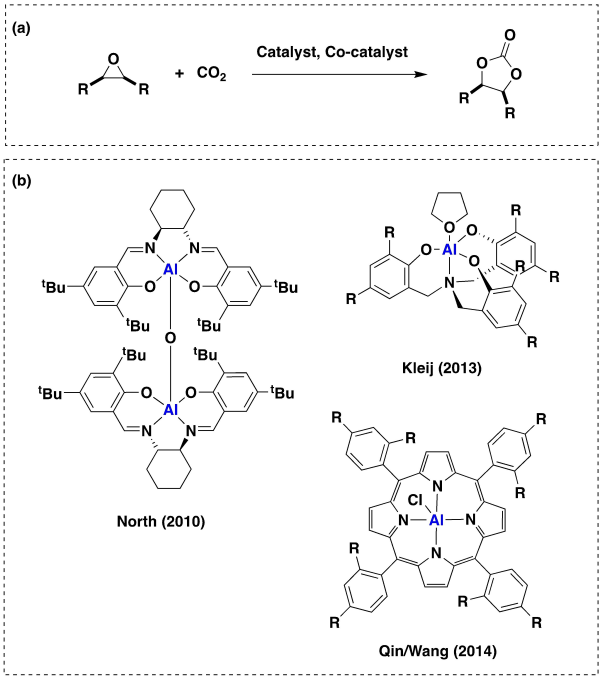

Scheme 1. (a) General reaction of epoxides and CO_2 for the synthesis of cyclic carbonates. (b) Selected examples of highly active catalysts for the synthesis of cyclic carbonates based on aluminium.

[a] Dr. L. Álvarez-Miguel, J. D. Burgoa, Dr. M. E. G. Mosquera, Dr. C. J. Whiteoak
Department of Organic and Inorganic Chemistry
and Research Institute in Chemistry "Andrés M. del Río" (IQAR)
Universidad de Alcalá
Campus Universitario, 28871 Alcalá de Henares, Madrid (Spain)
E-mail: martaeg.mosquera@uah.es
christopher.whiteoak@uah.es
[b] Dr. A. Hamilton
Biomolecular Sciences Research Centre (BMRC)
and Department of Biosciences and Chemistry
College of Health, Wellbeing and Life Sciences
Sheffield Hallam University
Howard Street, Sheffield, S1 1WB (United Kingdom)
E-mail: a.hamilton@shu.ac.uk

Supporting information for this article is available on the WWW under https://doi.org/10.1002/cctc.202100910

epoxide substrates through a Lewis pair interaction, arising from the use of a Lewis acid catalyst and the lone-pair of the oxygen from the epoxide, which results in a state that facilitates the key ring-opening of the epoxide by an external nucleophile co-catalyst.[8] The use of group 13 compounds as Lewis acids is very well established and therefore it is not unexpected that some of the most active catalysts known for the synthesis of cyclic carbonates are based on aluminium (Scheme 1b).[9] What is surprising however, is the relative lack of other group 13 elements being studied as the basis for catalysts; there are actually very few examples of boron compounds for this application, with a small number of groups reporting on the utility of aryl/alkyl-boranes as catalysts in 2019 and 2020.[10,11]

Meanwhile, Shibata (2011)[12] and more recently Hein/Mehrkhodavandi (2021)[13] have both described the use of indium bromide as catalyst.[14] Aside from these notable reports, to the best of our knowledge, no successful gallium-based catalyst systems have been described to date,[15] despite gallium triflate being well known as a Lewis acid catalyst[16] and a range of gallium complexes being described as catalysts for ring-opening polymerization of cyclic ethers, esters and carbonates.[17]

Compounds incorporating the aminotrisphenol ligand have been reported for a wide range of applications[18] and the highly active aluminium catalyst for synthesis of cyclic carbonates reported by Kleij in 2013[9b] (Scheme 1b) is based on this privileged ligand scaffold. In the context of this work, Kleij and Kleij/Licini have also reported on both iron(III) and vanadium(V) catalysts based on the same ligand scaffold as catalysts for the synthesis of cyclic carbonates.[19,20] Returning to gallium, in 1998 Martell/Koch reported on the first synthesis and characterization of gallium aminotrisphenolate compounds,[21] although no further application was sought. Thereafter, in 2007, Singh reported on similar compounds using a more facile synthetic approach, however, again with no application of the synthesized compounds.[22] With these two latter reports in mind, we decided to synthesize the gallium aminotrisphenolate compounds and explore their potential application as catalysts for the synthesis of cyclic carbonates from epoxides and CO_2. Herein, the results of this experimental investigation are disclosed in combination with important insights gained from an in-depth computational investigation into the direct comparison of these gallium compounds and their aluminium congeners.

Results and Discussion

Initially, the synthesis of **GaL^{x}** (X = Me and Cl) was realized (Scheme 2a) using a slightly modified approach to that reported by Singh;[22] reaction of the pro-ligand with $Ga(OEt)_3$ in toluene at 110 °C overnight resulted in the desired gallium aminotrisphenolate compounds in high yield and analytical purity. Compounds based on both **H_3L^{Me}** and **H_3L^{Cl}** were utilized given the precedence for the higher activity of the **AlL^{Cl}** compared with **AlL^{Me}** when applied as catalysts for the synthesis of cyclic carbonates.[23] It should be noted that the synthesis of the

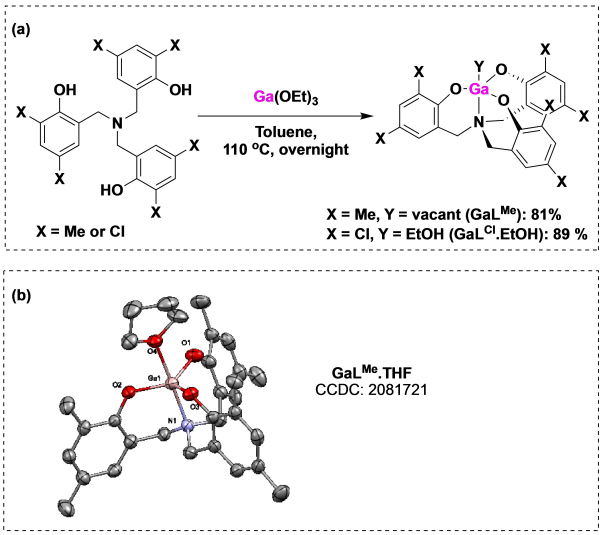

Scheme 2. (a) Synthesis of gallium aminotrisphenolate compounds to be used as catalysts. (b) X-ray structure of the gallium compound obtained from **H_3L^{Me}** (hydrogen atoms omitted for clarity).

gallium congeners reported uses $Ga(OEt)_3$ as precursor and therefore the synthetic procedure can be carried out under air and without the necessity to use anhydrous solvents or an inert atmosphere, unlike the aluminium compounds which use air and moisture sensitive $AlMe_3$ as reagent. Upon isolation of the **GaL^{Me}** and **GaL^{Cl}** compounds, it was observed that the latter compound contained an associated ethanol molecule and was actually better described as **GaL^{Cl}.EtOH**. The ethanol ligand can however be readily substituted for THF by dissolving in THF and removing the solvent under vacuum, indicating both the Lewis acid character and the potential for ligand exchange, which is essential for catalysis to proceed (see Supporting Information for spectra of this exchange). In contrast to **GaL^{Cl}.EtOH**, the gallium compound obtained from **H_3L^{Me}** does not contain an associated ethanol molecule or any other ligand in the apical position, as confirmed by inspection of the ^{1}H NMR spectrum. It was possible to obtain crystals suitable for X-ray crystallography studies of both of these gallium compounds (for the structure obtained for **GaL^{Me}** see Scheme 2b; for the structure of **GaL^{Cl}.EtOH** see Supporting Information), where in the case of **GaL^{Cl}.EtOH** the ethanol ligand has exchanged with a molecule of water during the crystallization process and as a result of the crystalizing medium, **GaL^{Me}** was obtained with an associated THF molecule indicating the possibility of coordination of Lewis bases to this compound.

With both gallium aminotrisphenolate compounds in hand, studies into their potential to catalyse the synthesis of the cyclic carbonate derived from 1,2-epoxyhexane and 8 bar CO_2 were initiated (Table 1) at room temperature using a binary catalyst system approach (catalyst + ammonium halide salt). Pleasingly, after only 4 hours at 15 °C both the **GaL^{Me}** and **GaL^{Cl}.EtOH** compounds were found to achieve 23 and 28% of the cyclic carbonate product respectively using tetrabutylammonium iodide (TBAI) as co-catalyst (Table 1, entries 1 and 2). It is

Table 1. Optimization of reaction conditions using gallium aminotrisphenolate catalysts and comparison with aluminium aminotrisphenolate congeners at 15 and 90 °C.[a]

Entry	Catalyst [mol%]	Co-catalyst [mol%]	*t* [h]	Yield [%][b,c]
Reactions at 15 °C				
1	**GaL^{Me}**, 0.25	TBAI, 1.25	4	23
2	**GaL^{Cl}.EtOH**, 0.25	TBAI, 1.25	4	28
3	**AlL^{Me}.THF**, 0.25	TBAI, 1.25	4	9
4	**AlL^{Cl}.THF**, 0.25	TBAI, 1.25	4	13
5	**GaL^{Me}**, 0.25	PPNCl, 1.25	4	0
6	**GaL^{Me}**, 0.25	TBAB, 1.25	4	21
7	**GaL^{Me}**, 0.25	TBAI, 1.25	16	87
8	**GaL^{Cl}.EtOH**, 0.25	TBAI, 1.25	16	91
9	**GaL^{Me}**, 0.5	TBAI, 2.5	16	>99
10	**GaL^{Me}**, 0.5	TBAI, 2.0	16	>99
11	–	TBAI, 2.0	16	trace
Reactions at 90 °C				
12	**GaL^{Me}**, 0.02	TBAI, 0.08	16	87
13	**GaL^{Cl}.EtOH**, 0.02	TBAI, 0.08	16	80
14	**GaL^{Me}**, 0.025	TBAI, 0.1	16	>99
15	**AlL^{Cl}.THF**, 0.025	TBAI, 0.1	16	79
16	–	TBAI, 0.1	16	trace
17	**GaL^{Me}**, 0.00025	TBAI, 0.05	70	86 (344,000)[d]
18	**GaL^{Me}**, 0.5	TBAI, 2.0	2	>99

[a] General reaction conditions: 1,2-epoxyhexane (1.0 g, 9.98 mmol), catalyst, co-catalyst, time, 15 or 90 °C, CO_2 (8 bar, sealed reactor). [b] Yield determined by ^{1}H NMR spectroscopy using mesitylene as internal standard. [c] Selectivity in all cases is >99% for the cyclic carbonate product. [d] Value in parenthesis relates to the turnover number (TON) obtained based on the catalyst loading. TBAI = tetrabutylammonium iodide; TBAB = tetrabutylammonium bromide; PPNCl = bis(triphenylphosphine)iminium chloride.

notable that these results were obtained with a relatively low catalyst loading of 0.25 mol% and TBAI loading of 1.25 mol%. We were curious to compare this result to the aluminium congeners, where it was found that at this early point of our studies, the gallium catalysts exhibited improved activities under these conditions (Table 1, entries 1 and 2 *vs.* entries 3 and 4).

With the knowledge that the gallium compounds were capable of catalysing the reaction, we then proceeded to fully optimize the gallium binary catalyst system. **GaL^{Me}** was chosen as the catalyst to optimize as a result of the ligand being much easier to synthesize, despite initial experiments showing that **GaL^{Cl}.EtOH** displays slightly higher catalytic activity. When using **GaL^{Me}** and 4 hours of reaction time, both bis(triphenylphosphine)iminium chloride (PPNCl) and tetrabutylammonium bromide (TBAB) provided lower product yields than TBAI (Table 1, entries 5 and 6 *vs.* entry 1). Increasing the time from 4 to 16 hours, under the same catalyst and co-catalyst loadings, resulted in an increase in yield to 87% (Table 1, entry 7), where again **GaL^{Cl}.EtOH** only provided a slightly higher yield compared to **GaL^{Me}** (Table 1, entries 7 and 8). Doubling of the catalyst loading (to 0.5 mol%) and increasing the co-catalyst loading to 2.0 mol% allowed for a yield in excess of 99% (Table 1, entry 10) and the final optimized conditions at room temperature. Under these conditions, omission of the gallium compound resulted in only trace observation of the cyclic carbonate product (Table 1, entry 16).

In addition to optimizing the binary catalyst system at room temperature, a similar optimization was realized at 90 °C and 8 bar CO_2 pressure with the aim of being able to apply much lower catalyst loadings. Reducing the loading of **GaL^{Me}** to 0.02 mol% and TBAI loading to 0.8 mol% resulted in a yield of 87% after 16 hours of reaction at this elevated temperature (Table 1, entry 12) which was in this case actually higher than when **GaL^{Cl}.EtOH** was used (Table 1, entry 13; 80%). Slight increase of the catalyst and TBAI loading to 0.025 and 0.1 mol% respectively, resulted in a quantitative conversion (Table 1, entry 14), which is much higher than obtained using **AlL^{Cl}.THF** under the same conditions (Table 1, entry 15; 79%), providing further experimental evidence for the higher activity of the gallium congeners. Again, under the optimized conditions, omission of the gallium catalyst resulted in only trace cyclic carbonate product (Table 1, entry 16). Finally, the potential Turn-Over-Number (TON) was explored, where it was found that when using a reduced binary catalyst system at loadings of 0.00025 mol% **GaL^{Me}** and 0.05 mol% TBAI for an extended reaction period of 70 hours at 90 °C and 8 bar CO_2 pressure, 86% product was obtained, which equates to a TON of 344,000 per catalyst molecule, indicating that the catalyst system exhibits high stability. Finally, to exemplify that the catalyst system can be applied under shorter reaction times, an experiment using both elevated catalyst system loading, and temperature was attempted (Table 1, entry 18). Indeed, within 2 hours it was possible to obtain complete conversion under these conditions. In summary, the developed catalyst system can be applied at both ambient and elevated temperatures, with the advantage of reduced catalyst system loading in the latter.

Additionally, short reaction times can be used if a high catalyst loading at elevated temperature is applied.

With an optimized binary catalyst system developed at both room temperature and 90 °C, at 8 bar CO_2 pressure, the substrate scope was studied under both of these conditions (Tables 2 and 3). During both of these investigations, yields were obtained based on ^{1}H NMR of the crude reaction mixture using mesitylene as internal standard and the cyclic carbonate products were thereafter purified by column chromatography. With the aim of achieving the highest conversions possible, in some cases increased catalyst/co-catalyst loadings, change to TBAB (smaller nucleophile) co-catalyst or extended reaction times were applied as a deviation from the optimised reaction conditions (see table footnotes for details).

At 15 °C it was possible to convert a range of terminal epoxides to the corresponding cyclic carbonates in good to quantitative yields (Table 2, cyclic carbonates **1a**–**14b**). It should be noted that glycidol is a special case, the double role of substrate and catalyst, through hydrogen bonding interactions, for this substrate has been previously studied by Capacchione.[24] Under our experimental conditions, in the presence of TBAI alone, glycidol (**6a**) was converted in 60% yield to the corresponding cyclic carbonate product, **6b**. To achieve the complete conversion under the co-catalyst loadings used here, the gallium catalyst is therefore required. When internal or 1,1-substituted epoxides were used as substrates, generally poor yields were obtained and in the case of cyclohexene oxide (**16a**), polycarbonate was clearly observed in the ^{1}H NMR spectrum of the crude reaction mixture (see Supporting Information, Figure S74). We were unable to recover any meaningful quantity of cyclic carbonate from this reaction as the product is predominantly polycarbonate/polyether with only trace cyclic carbonate present (28% yield). Interestingly, previously Darensbourg has, without success, reported on attempts to apply gallium Salen compounds as catalysts for the synthesis of polycarbonates from cyclohexene oxide.[25] It is therefore clear that at room temperature the binary catalyst

Table 2. Substrate scope using **GaL^{Me}** catalyst at 15 °C.[a,b]

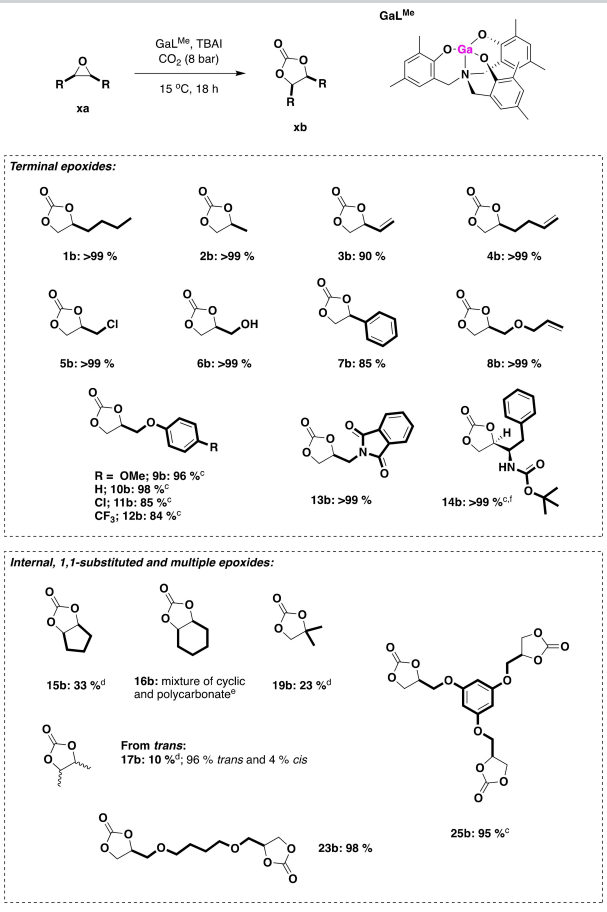

[a] General conditions: Epoxide, **GaL^{Me}** (0.5 mol%), TBAI (2.0 mol%), 15 °C, CO_2 (8 bar, sealed reactor), 18 h. [b] NMR yields reported. [c] 2-butanone used as co-solvent. [d] TBAB used in place of TBAI due to improved yield of cyclic carbonate. [e] See Supporting Information for ^{1}H NMR spectrum of the crude reaction mixture: Figure S74; the mixture predominately contains polycarbonate and polyether. [f] 72 h reaction time.

Table 3. Substrate scope using **GaL^{Me}** catalyst at 90 °C.[a,b]

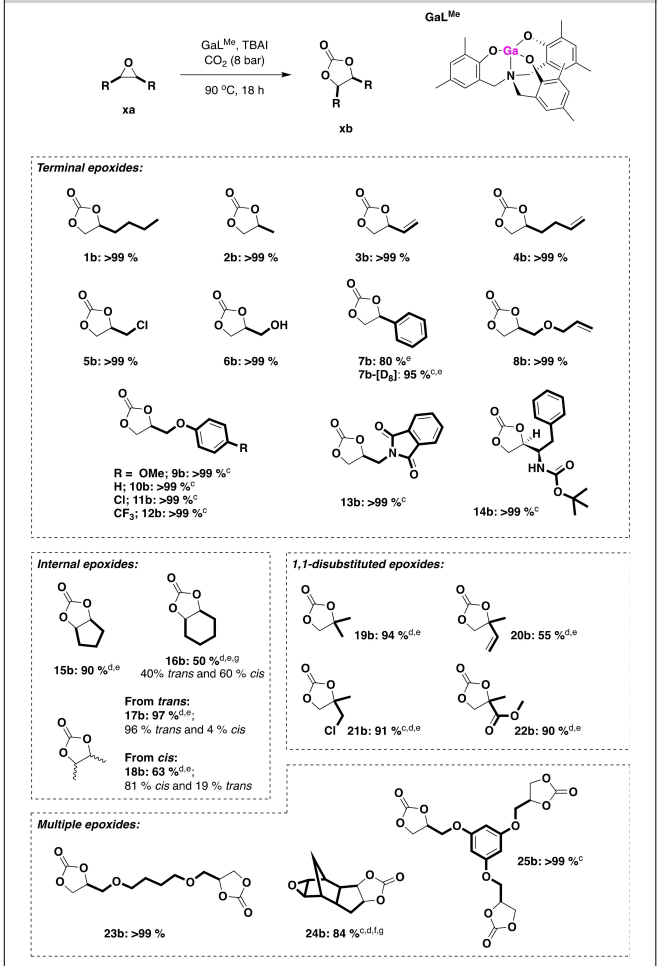

[a] General conditions: Epoxide, **GaL^{Me}** (0.025 mol%), TBAI (0.1 mol%), 15 °C, CO_2 (8 bar, sealed reactor), 18 h. [b] NMR yields reported. [c] 2-butanone used as co-solvent. [d] TBAB used in place of TBAI due to improved yield of cyclic carbonate. [e] 0.1 mol% **GaL^{Me}** and 0.4 mol% co-catalyst used. [f] 0.25 mol% **GaL^{Me}** and 0.4 mol% co-catalyst used. [g] 68 h reaction time. [h] See Supporting Information for ^{1}H NMR spectrum of the crude reaction mixture: Figure S75.

system is only suitable for conversion of terminal epoxides. As a further development of this, products were then successfully obtained containing multiple terminal cyclic carbonates (Table 2, **23b** and **25b**) in excellent yields. Compounds bearing multiple cyclic carbonates are currently of particular interest for the synthesis of non-isocyanate polyurethanes (NIPU's), with **25b** being of interest for the synthesis of highly complex three-dimensional NIPU's which may offer novel/improved properties over simple linear analogues.[26] To the best of our knowledge this is the first time this compound has been prepared.

With the substrate scope completed at room temperature, a study was carried out under the optimized reaction conditions at 90 °C (Table 3). Again, as with the room temperature study, generally quantitative yields were obtained with terminal epoxide (Scheme 4, **1b**–**14b**) and the terminal multiple epoxide substrates (Table 3, **23b** and **25b**). Glycidol (**6a**) without gallium catalyst was auto catalysed with a yield of 65% in similarity to the results obtained at 15 °C, again indicating the necessity for catalyst to achieve complete conversion at this low TBAI loading (0.1 mol%).

In contrast to the room temperature study, cyclopentene oxide (Table 3, **15b**) and also the 2,3-epoxybutanes (both *cis* and *trans*) could be converted, with the latter showing stereochemical inversions and retentions similar to those reported by Kleij for the iron(III) aminotrisphenolate catalysts under high co-catalyst loading.[27] Cyclohexene carbonate (Table 3, **16b**) was also obtained, however, again the crude reaction mixture clearly contains small amounts of polycarbonate species (44% yield of cyclic carbonate with only traces of polycarbonate/polyether), although purification of the cyclic carbonate product was possible this time. In this product, a mixture of both *cis*- and *trans*-cyclic carbonates were observed (60:40), with the latter likely arising from backbiting of the polycarbonate chain.[28] In addition to internal epoxides, a range of challenging 1,1-substituted epoxides could also be successfully converted to the corresponding cyclic carbonate products in good to excellent yields (Table 3, **19b**–**22b**). It should be noted that the reduced yield of **20b** is a result of an unidentifiable side product being generated during the reaction which is not surprising given the high reactivity of this product. Finally, an epoxide based on dicyclopentadiene was successfully converted to the corresponding cyclic carbonate where only one of the epoxides is selectively converted (Table 3, **24b**). This selectivity has previously been observed by the few groups that have attempted conversion of this challenging substrate.[5b,20,29,30] In summary, increasing the reaction temperature, allows for the successful conversion of more complex substrates. Of further note is the ability to synthesize a fully deuterated analogue of **7b**, **7b**-[D_8], which to the best of our knowledge is the first time this compound has been prepared. This cyclic carbonate was readily synthesized from the deuterated styrene oxide, **7a**-[D_8][31] in similar yield to the non-deuterated analogue. This compound may be of particular interest for synthesizing fully deuterated polycarbonates[32] which can be used for polymer neutron diffraction studies. Fully deuterated propylene carbonate has already been used in various neutron diffraction studies, highlighting the potential of deuterated cyclic carbonates in advanced analysis techniques.[33]

Our next steps were to obtain more information about the mechanism of the conversion in the context of the comparison of the newly developed binary gallium catalyst system with the previously reported aluminium congeners. First, experimental data was obtained concerning the Lewis acid nature of both gallium and aluminium aminotrisphenolate compounds bearing both $\mathbf{L^{Me}}$ and $\mathbf{L^{Cl}}$ ligands through the Gutmann-Beckett Method (Figure 1).[34] The $^{31}P\{^1H\}$ NMR spectra obtained for all the complexes clearly show that the Lewis base employed (Et_3PO) coordinates to both the gallium and aluminium compounds to form the Lewis pair and therefore allows for the calculation of the Acceptor Number (AN). In all cases it was found that the gallium congener is more Lewis acidic than the corresponding aluminium compound when using the same ligand (increased AN).

Meanwhile, it is also observable that the in the case of both gallium and aluminium the use of $\mathbf{L^{Cl}}$ instead of $\mathbf{L^{Me}}$ results in a compound with increased Lewis acidity (increased AN). When comparing the order of Lewis acidity and relative catalytic performance (Table 1, entries 1–4 and Figure 1) it is clear that Lewis acidity is not the only factor to be considered, as taking the obtained AN's and correlating them against catalytic activity does not explain why $\mathbf{GaL^{Me}}$ displays a higher activity than $\mathbf{AlL^{Cl}.THF}$, which is clearly more Lewis acidic in nature. After a more detailed inspection of the obtained NMR spectra an unexpected broadening of the signal corresponding to the $\mathbf{Et_3PO\text{-}GaL^{Me}}$ Lewis pair is observed. This broadening is not present in any of the other compounds investigated and can be assigned to a more rapid exchange of Et_3PO compared with the other compounds studied. From an experimental point of view, it would therefore appear that this increased rate of exchange is of benefit for the catalysis process and provides evidence that during catalyst development, Lewis acidity is not the only variable that should be considered when attempting to generate a highly active catalyst.

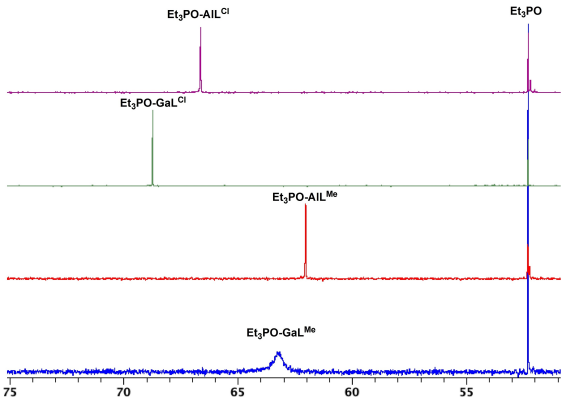

Figure 1. $^{31}P\{^1H\}$ spectra (298 K) obtained from measurement of the Lewis acid Acceptor Number (AN) using the Gutmann-Beckett method (Et_3PO, $CDCl_3$). Calculated AN's: $\mathbf{GaL^{Me}}$ = 63.23 (broad, fluxional); $\mathbf{AlL^{Me}.THF}$ = 62.02; $\mathbf{GaL^{Cl}.EtOH}$ = 68.72; $\mathbf{AlL^{Cl}.THF}$ = 66.83.

To further investigate this unexpected ordering of the metal Lewis acidity theoretical Fluoride Ion Affinity (FIA) calculations were performed using the TMS-anchored isodesmic reaction method proposed by Greb[35] (see experimental section for full details). From Table 4 it is clear that these methods, based on reaction enthalpies, are inconsistent with the experimental data obtained using the Gutmann-Beckett method. The non-ligated reaction shows the aluminium congeners to be more Lewis acidic than the corresponding gallium compounds, as would generally be expected for simpler systems, however, it is not correct for the system in this work. Meanwhile, the ligand substitution reaction shows **GaL^{Me}** to be most Lewis acidic. This latter interaction, although closer to the experimental reaction, is not isodesmic and the use of reaction enthalpies does not account for entropic contributions. A more isodesmic ligated reaction leads to a closer match to the experiments, however the relative **AlL^{Cl}.THF** and **GaL^{Cl}.EtOH** FIA values are still inconsistent. Additionally, these fluorinated complexes are not overly representative of experimental species in this system. It should be noted that the values for **GaL^{Me}** are the same under all three studies as there is no ligand present in the structure. To understand the Gutmann-Beckett results in more detail we calculated the theoretical ^{31}P NMR chemical shifts (see experimental section for details) using **OPMe$_3$** as a reference for calculating the theoretical AN values. The ordering of the AN of the 4 species agrees with the experimental values (Figure 1 *vs.* Table 4). Further to this, electron density at the line critical point (*lcp*) between phosphorus and oxygen for each of the species was calculated with Quantum Theory of Atoms In Molecules (QTAIM) and the results provide excellent agreement with the Lewis Acidity derived from the Gutmann-Beckett method, with the calculated electron density for **Me$_3$PO-GaL^{Cl}** showing the greatest derivation from free **OPMe$_3$**, and therefore the greatest Lewis acidity.

Thereafter, in an attempt to further understand the reactivities observed for the **GaL^{Cl}** and **GaL^{Me}** catalysts, and compare this directly to the aluminium congeners, we undertook a comprehensive computational mechanistic investigation. There have been numerous previous studies on a wide range of catalyst systems for the synthesis of cyclic carbonates from epoxides and CO_2.[36] and indeed, the mechanism for the aluminium aminotrisphenolate catalysed reaction has already been reported.[23] In this original study, Kleij and Bo proposed the energy span for the aluminium-based catalyst to be ~34 kcal mol^{-1}. However, this mechanism was subsequently re-evaluated, including isomerisation between the α and β-CO_2 insertion pathways and different methods of assessing the entropic contribution, leading to reduced energy spans of 21.8 kcal mol^{-1} (ωB97XD/6-311G(d,p)/LANL2DZ), in excellent agreement with the experimental Turn-Over-Frequency (TOF) data.[37] Using this work as a starting point we elucidated the operative mechanism for both the **GaL^{Cl}** and **GaL^{Me}** catalysts, at the ωB97M–D3BJ/def2-tzvpp level of theory, as well as computing the energy span for the aluminium congeners with the same method. Prior to full mechanistic elucidation the structure of the respective initial catalysts was determined. Experimental evidence shows the coordination of an ethanol molecule to **GaL^{Cl}**, whilst the **GaL^{Me}** catalyst appears to have a vacant apical coordination site. The DFT calculations are in agreement with the experimental observations with an ethanol coordinated to **GaL^{Cl}** being favourable by −3.7 kcal mol^{-1}, while binding of the same ligand to **GaL^{Me}** being unfavourable by 2.7 kcal mol^{-1}. From this point these structures were used as the initial catalysts.

As expected, the mechanism follows a similar pathway to that of the aluminium congeners previously reported (Figure 2). Initial binding of the epoxide to the catalyst forms, **IC**. In this step the **GaL^{Cl}.EtOH** catalyst requires displacement of the transient ethanol molecule, whereas with **GaL^{Me}** no such exchange is necessary. The concentration corrected relative energies for these intermediates, compared to the initial catalyst structures, are −2.5 kcal mol^{-1} and −2.1 kcal mol^{-1} respectively, and are shown to be the Turnover Determining Intermediate's (TDI's) for the reaction. The expected stronger binding energy for **GaL^{Cl}** is clearly observed (−6.4 kcal mol^{-1} compared to the uncoordinated catalyst), however, there is an energy penalty for displacing the coordinated ethanol molecule and indeed, in subsequent catalytic cycles this will be transient solvent from the reaction. The epoxide ring opening step, **TS1**, occurs through iodide mediated breaking of the C_β-O bond and simultaneous formation of a C_β-I bond, by the TBAI co-catalyst, with a barrier of 9.7 kcal mol^{-1} for **GaL^{Cl}** and 12.2 kcal mol^{-1} for **GaL^{Me}** catalysts. The subsequent metal-alkoxide intermediate, **Int1**, is energetically less stable than the preceding intermediate, **IC**, with a $\triangle\triangle G_{298K}$ between **GaL^{Cl}** and **GaL^{Me}** of 4.2 kcal mol^{-1}. This trend of **GaL^{Cl}** being consistently more stable compared to **GaL^{Me}** is seen throughout the calculated reaction mechanism. From **Int1** there are two pathways by which the CO_2 can insert into the Ga–O bond. The α-pathway, axial approach, is less favourable than the equivalent equatorial β-pathway, by $\triangle\triangle G_{298K} = 3.2$ kcal mol^{-1} and 7.2 kcal mol^{-1} for **GaL^{Cl}** and **GaL^{Me}** respectively. The β-pathway barriers heights, **TS2$_\beta$**, are 21.4 kcal mol^{-1} and 23.2 kcal mol^{-1} for are **GaL^{Cl}** and **GaL^{Me}** respectively, relative to **IC**, the TDI for each mechanism. The

Table 4. Calculated FIA values (kJ mol^{-1}), calculated Gutman-Beckett AN values and change in P–O *lcp* electron density (ρ) on formation of a **catalyst-OPMe$_3$** Lewis pair.

	Fluoride Ion Affinity [kJ mol^{-1}]			Gutmann-Beckett	
	Non-ligated	Substitution	Isodesmic ligated	Calc. AN	$\Delta\rho$(P–O) ($\times 10^{-2}$)
GaL^{Cl}	384.7	300.6	344.7	73.5	2.04
AlL^{Cl}	419.2	309.1	355.9	71.2	1.96
GaL^{Me}	323.1	323.1	323.1	61.7	1.66
AlL^{Me}	361.5	273.3	305.3	60.2	1.64

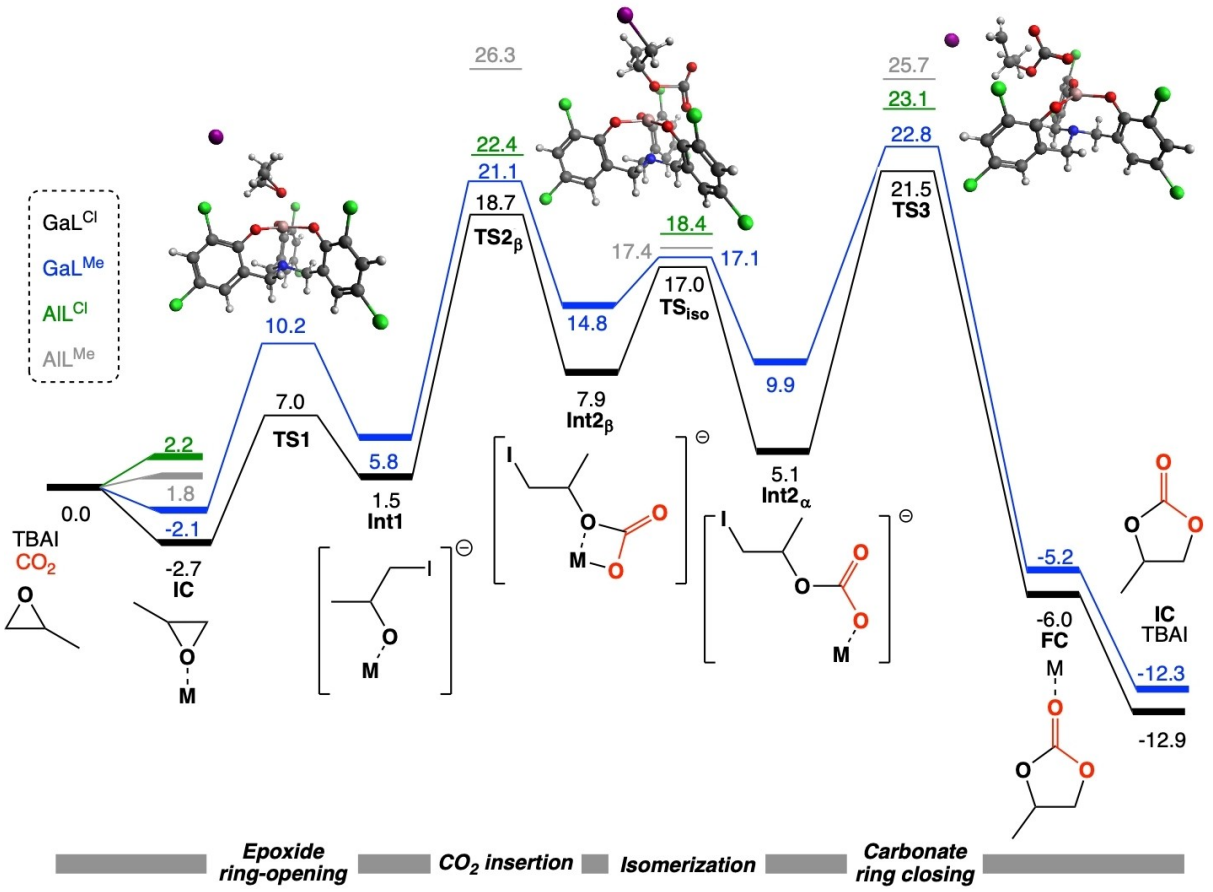

Figure 2. Calculated free energy surface (ΔG_{298K}), ωB97M-D3BJ/def2-tzvpp, for cyclic carbonate synthesis using propylene oxide as substrate with **GaL^{Cl}** (black line) and **GaL^{Me}** (blue line). Energies for key intermediates and transition states in the mechanism using **AlL^{Cl}** (green line) and **AlL^{Me}** (grey line) are also shown. Shown calculated geometries relate to **TS1**, **TS2$_\beta$** and **TS3** along the **GaL^{Cl}** pathway.

following intermediates, **Int2$_\beta$**, in the linear carbonate form can undergo isomerization, *via* **TS$_{iso}$**, to the more stable **Int2$_\alpha$**. The barriers for these isomerization steps are 9.1 kcal mol^{-1} and 2.3 kcal mol^{-1} for **GaL^{Cl}** and **GaL^{Me}** respectively. The lower **GaL^{Me}** barrier is due to the less stable **Int2$_\beta$** rather than a stabilization of the transition state structure. Continuation of the reaction mechanism *via* the stabilized linear carbonate intermediate, **Int2$_\alpha$**, affords a ring closure transition state, **TS3**, with C–O bond formation and synchronous C–I bond breaking. For both **GaL^{Cl}** and **GaL^{Me}** systems **TS3** is the highest barrier on the free energy surface, and therefore is identified as the TOF-Determining Transition State (TDTS) for the reaction, in agreement with previous work on the equivalent **AlL^{Cl}** system. For **GaL^{Cl}** an equivalent ring closure step was calculated from **Int2$_\beta$** however this was shown to be 5.6 kcal mol^{-1} higher in energy. Finally, **TS3** leads to the cyclic carbonate product coordinated to the catalyst, **FC**, which can then exchange with another molecule of epoxide, closing the catalytic cycle. The energy span for both catalytic systems is identified from **IC** to **TS3** and gives values of 24.2 kcal mol^{-1} and 24.8 kcal mol^{-1} for **GaL^{Cl}** and **GaL^{Me}** respectively. The equivalent energy spans for the **AlL^{Cl}** and **AlL^{Me}** catalytic systems, calculated at the same level of theory, are 23.1 kcal mol^{-1} and 26.3 kcal mol^{-1}. These **AlL^{Cl}** catalyst values are similar to those previously reported,[36] although differ slightly due to the computational methodology used and identification of the TDI. Interestingly, previously reported energy span models highlighted the **IC** intermediate as the TDI for the aluminium congeners, whereas calculations from this study suggest the initial catalyst-THF adduct is more stable by approximately 2.0 kcal mol^{-1} for both systems. To the best of our knowledge the catalyst-THF adduct was not included in previously calculated mechanisms, with the reaction starting from the aluminium catalyst with a vacant coordination site. Pleasingly the overall energy spans and trends across the four catalytic systems are in reasonable agreement with the experimental findings, particularly highlighting the impressive performance of the **GaL^{Me}** catalyst. It should be noted that the AlICl catalyst gives the lowest overall energy span (TDI→TDTS, see Figure 2), contrary to the experimental evidence, both **GaL^{Me}** and **GaL^{Cl}** have overall lower energy requirements starting from their respective initial catalyst structure. This brings to light the question if static energetics, and energy spans, are enough to fully understand complex catalytic reactions; a point recently raised in a related catalytic system by Kerton.[38]

The experimentally observed broadening of the peak for the **OPEt$_3$·GaL^{Me}** complex in the $^{31}P\{^1H\}$ NMR spectrum suggests potential increased dynamic behaviour of this catalyst. To try and quantify this dynamic behaviour we performed Ab-Initio Molecular Dynamic (AIMD) simulations using the recently published GFN2-xTB semi-empirical tight-binding based quantum chemistry method.[40] This functional has been shown to reproduce excellent structural parameters for a range of molecular systems, from complex organic species, bulky organometallic complexes through to protein systems.[40] Molecular Dynamic (MD) simulations with the GFN2-xTB functional has seen application in exploration of conformer and reaction space.[41] The benefit of using the GFN2-xTB functional for MD simulations is the access to longer simulation times without the need to derive specialist force fields for Molecular Mechanics (MM) based MD simulations.

MD simulations for **IC** with the all the gallium and aluminium compounds were performed to evaluate the dynamics of the metal-epoxide interaction, as well as the internal metal-amine interaction with the aminotrisphenolate ligand. For each complex the structure was allowed to equilibrate for 25 ps at 298 K (50,000 steps with 0.5 fs step size), followed by a further 25 ps production run. Figure 3 shows the variation in the M–O and M–N bond distances over the production run timescale, with descriptive statistics provided in Table 5. What is evident from the simulations is the increased dynamic behaviour within the **GaL^{Me}** catalyst, showing a greater M–O bond length variance and standard deviation compared to the other

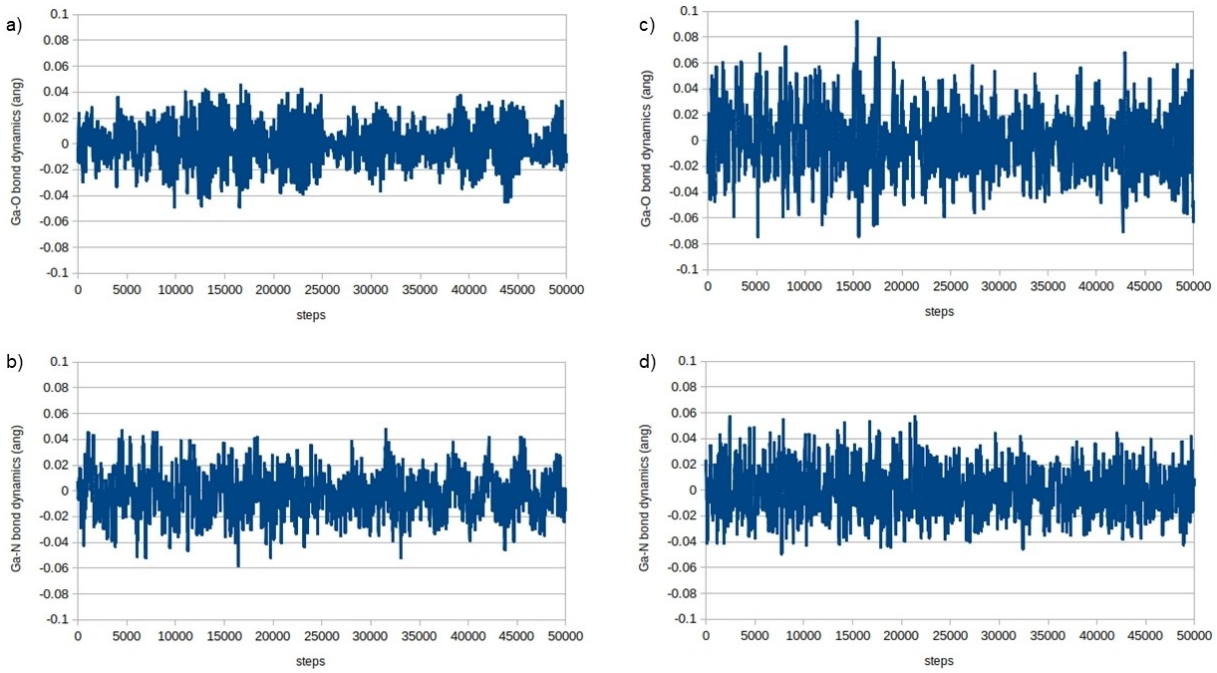

Figure 3. Variation in bond length for the duration for AIMD simulation (25 ps). a) **GaL^{Cl}** Ga–O bond; b) **GaL^{Cl}** Ga–N bond; c) **GaL^{Me}** Ga–O bond; d) **GaL^{Me}** Ga–N bond.

Table 5. Descriptive statistics obtained from the MD simulations.

	GaL^{Me} Ga–O	Ga–N	**GaL^{Cl}** Ga–O	Ga–N
Mean Bond Length [Å]	2.12	2.17	2.03	2.22
Standard Error ($\times 10^{-3}$)	0.24	0.17	0.14	0.59
Variance ($\times 10^{-3}$)	2.87	1.51	1.05	1.76
Standard Deviation ($\times 10^{-2}$)	5.36	3.89	3.32	4.19
Range [Å]	0.35	0.23	0.19	0.20
	AlL^{Me} Ga–O	Ga–N	**AlL^{Cl}** Ga–O	Ga–N
Mean Bond Length [Å]	1.95	2.19	1.87	2.23
Standard Error ($\times 10^{-3}$)	0.22	0.19	0.11	0.17
Variance ($\times 10^{-3}$)	2.32	1.86	0.59	1.52
Standard Deviation ($\times 10^{-2}$)	4.82	4.31	2.43	3.91
Range [Å]	0.32	0.31	0.16	0.23

catalysts (Table 5). The increased dynamics of the M–O bond is coupled with reduced variance in the M–N bond, suggesting for the **GaL^{Me}** catalyst the metal is bound in a stronger fashion to the amine donor, therefore reducing the epoxide interaction allowing for faster axial ligand exchange.

To further quantify these M–O and M–N interactions we have undertaken QTAIM topological analysis on the four IC complexes. Notably, the line critical points, *lcp*, for the M–N interactions (Table 6) for **IC** of **GaL^{Me}** highlight significantly greater electron density ($\rho(r_c)$; a descriptor of bond strength) compared to the other catalysts, further confirming the observations and conclusions made from the MD simulations. The specific nature of the M–N interaction can be further described by the associated QTAIM parameters. In all cases the M–N interactions fall into the category of intermediate strength interaction. Positive values of $\nabla^2\rho(r_c)$ suggest an ionic/closed shell interaction, which can be decomposed into the corresponding kinetic energy density, $G(r_c)$, and electronic potential energy density, $V(r_c)$, terms. Summation of $G(r_c)$ and $V(r_c)$ terms gives the energy density, $H(r_c)$, which is an unambiguous descriptor of bond character. The negative value for $H(r_c)$, shows the potential energy density term dominating the bonding characteristic and therefore covalent nature of the bond. The $H(r_c)$ term is significantly greater for the gallium catalysts, and largest for **GaL^{Me}**, showing stronger, more covalent character. This discrepancy in bonding description, classified as partially covalent,[42] between $\nabla^2\rho(r_c)$ and $H(r_c)$ is well documented for amine L-type ligand interactions[43] and the calculated molecular orbital (HOMO-6) for this interaction is shown in Figure 4. Interestingly, a change in sign for $H(r_c)$ for the M–O interaction between the metal centres highlights a more closed shell ionic character (positive $H(r_c)$) for the aluminium catalysts. This difference in bonding character may account for the differing stabilities seen for the **IC** complexes.

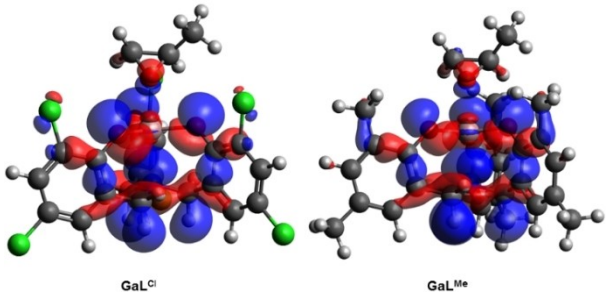

Figure 4. Calculated molecular orbitals highlighting the Ga–N interaction.

Conclusion

In conclusion, we have developed the first gallium-based catalyst system for the synthesis of cyclic carbonates from epoxides and CO_2. The catalyst system displays high activity and is demonstrated to be more active than catalyst systems based on the aluminium congeners of the same structure that have previously been reported. The developed catalyst system provides an impressive substrate scope, including those based on internal and multiple epoxide substrates. An in-depth computational study has been performed where the calculated reaction mechanism is in good agreement with experimental evidence and previous computational studies. The **GaL^{x}** (x = Me or Cl) catalysts show lower energetic profiles compared to the aluminium congeners. Key details of the mechanism have been fully explored and AIMD simulations clarify and quantify the dynamic behaviour of the catalytic systems, highlighting the increase fluxionality of the **GaL^{Me}** catalyst, which explains the higher-than-expected activity beyond just Lewis acidity considerations. In addition, significant differences observed with the different computational approaches to predicting Lewis acidity, FIA *vs.* Gutmann-Beckett, highlights the care that must be taken with making predictions based on theoretical scales for complex systems. These one-dimensional descriptors may miss important interactions that govern observed reactivity. Finally, QTAIM topological analysis has quantified the nature of the metal-to-ligand and metal-to-substrate interactions. In summary, the results disclosed in this work should encourage other researchers to explore the potential of other group 13 catalysts beyond those based on aluminium for the synthesis of cyclic

Table 6. QTAIM analysis of the M–O and M–N bonds for the four **IC** complexes.

	GaL^{Me}		**GaL^{Cl}**	
lcp	Ga–O	Ga–N	Ga–O	Ga–N
$\rho(r_c)$	0.0534	0.0738	0.0632	0.0675
$\nabla^2\rho(r_c)$	0.2116	0.2222	0.2675	0.1896
$G(r_c)$	0.0601	0.0733	0.0765	0.0631
$V(r_c)$	−0.0674	−0.0909	−0.0862	−0.0787
$H(r_c)$	−0.0073	−0.0177	−0.0097	−0.0157
	AlL^{Me}		**AlL^{Cl}**	
lcp	Ga–O	Ga–N	Ga–O	Ga–N
$\rho(r_c)$	0.0443	0.0519	0.0503	0.0482
$\nabla^2\rho(r_c)$	0.2565	0.2181	0.2973	0.1953
$G(r_c)$	0.0625	0.0604	0.0733	0.0542
$V(r_c)$	−0.0618	−0.0663	−0.0722	−0.0592
$H(r_c)$	0.0017	−0.0059	0.0011	−0.0054

carbonates, and those based on gallium which remain rather dormant.

Experimental Section

All experimental procedures were carried out without the need to exclude air or moisture unless noted. All chemicals and solvents were purchased from Fisher or Merck and used without further purification. Ligands, **H_3L^{Me}** and **H_3L^{Cl}** and the aluminium catalysts, **AlL^{Me}.THF** and **AlL^{Cl}I.THF**, which were used for comparative purposes, were synthesized according to the literature procedures.[44] [D_8]-styrene oxide (**[D_8]-7a**) was synthesized from [D_8]-styrene according to the published procedure.[24] ^{1}H and ^{13}C{^{1}H} NMR spectra were obtained in $CDCl_3$ at 25 °C on a Bruker Avance 400 MHz spectrometer and referenced using the residual ^{1}H and ^{13}C resonances of the solvent. ^{31}P{^{1}H} NMR were referenced to 85% H_3PO_4 in aqueous solution. All catalytic reactions were performed in Berghof High-pressure reactors (BR-40, PTFE liner, 70 mL volume; see photo in the Supporting Information), using high-purity carbon dioxide (> 99.995%) purchased from Linde (no further purification), with an initial starting pressure of 8.0 bar.

Synthesis of gallium compounds

Synthesis of **GaL^{Me}**: To a round bottom flask containing **H_3L^{Me}** (629 mg, 1.50 mmol) and $Ga(OEt)_3$ (307 mg, 1.50 mmol) was added 20 mL of toluene. The flask was sealed, and the mixture heated to 110 °C with stirring overnight. The mixture was then cooled to room temperature, filtered through celite® and the solvent removed under vacuum. The resulting solid was then washed with hexane (2×15 mL) and finally dried under vacuum to provide **GaL^{Me}** as a white powder (592 mg, 81%). ^{1}H NMR (400 MHz, 298 K, $CDCl_3$) δ 6.92 (s, 3H, ArH), 6.62 (s, 3H, ArH), 3.84 (br s, 6H, $ArCH_2N$), 2.22 (s, 9H, CH_3), 2.18 (s, 9H, CH_3). ^{13}C{^{1}H} NMR (101 MHz, 298 K, $CDCl_3$) δ 155.66, 132.62, 129.03, 128.39, 127.89, 119.77, 58.72, 20.27, 16.42. HR-MS (ESI-TOF, m/z); calcd. for $C_{27}H_{30}GaNO_3+H=486.1560$; obtained = 486.1588 $[M+H]^+$. Crystals of the corresponding compound **GaL^{Me}.THF**, which were suitable for X-ray crystallography, were obtained by slow diffusion of hexane into a concentrated THF solution of **GaL^{Me}** and result from favourable incorporation of the THF ligand during the crystallization process. See: CCDC 2081721.

Synthesis of **GaL^{Cl}.EtOH**: This compound was prepared by the same procedure described for **GaL^{Me}** except **H_3L^{Cl}** (605 mg, 1.12 mmol) and $Ga(OEt)_3$ (229 mg, 1.12 mmol) were used. **GaL^{Cl}.EtOH** was obtained as a white powder (650 mg, 89%). ^{1}H NMR (400 MHz, 298 K, $CDCl_3$) δ 7.34 (s, 3H, ArH), 6.89 (s, 3H, ArH), 4.60 (m, 2H, EtOH), 3.70 (br s, 6H, $ArCH_2N$), 1.58 (m, 3H, EtOH). Ethanol is clearly interacting with the Ga as the chemical shifts in $CDCl_3$ are significantly changed from those of free ethanol. A poor quality ^{13}C{^{1}H} NMR spectrum was obtained using $CDCl_3$, so [D_6]-DMSO was used: ^{13}C{^{1}H} NMR (101 MHz, 298 K, [D_6]-DMSO) δ 156.63, 128.09, 127.81, 124.45, 123.24, 118.25, 58.58. HR-MS (ESI-TOF, m/z); calcd. for $C_{21}H_{12}Cl_6GaNO_3+H=605.8282$; obtained = 605.8294 $[M+H]^+$. Crystals of the corresponding compound **GaL^{Cl}.H_2O**, which were suitable for X-ray crystallography, were obtained by slow evaporation of a concentrated chloroform solution of **GaL^{Cl}.EtOH** and result from exchange of the ethanol ligand for a water ligand during the crystallization process. See: CCDC 2081027.

General Procedure for the Catalytic Conversion of Epoxides and CO_2 to Cyclic Carbonates using 1,2-epoxyhexane

A high-pressure reactor, equipped with a stirrer bar, was charged with catalyst, co-catalyst and 1,2-epoxyhexane (1.0 g, 9.98 mmol). The reactor was then filled with CO_2 to 2 bar and vented, a procedure that was repeated 3 times, before being finally filled with CO_2 to a pressure of 8 bar. The reactor was left stirring for the required time at the required temperature. At the end of the reaction the reactor was cooled and slowly vented before mesitylene (400 mg, 3.33 mmol) was added. An aliquot was then removed and dissolved in $CDCl_3$. The percentage conversion and NMR yield of the reaction was obtained from the ^{1}H NMR spectrum of this crude sample using the mesitylene as internal standard. The crude reaction mixture was then purified using column chromatography to provide analytically pure cyclic carbonate products.

Measurement of the Lewis Acid Acceptor Number (AN) using the Gutmann-Beckett Method[34]

This procedure was carried out in an argon-filled glove box; A 20 mM solution of the compound to be analysed was made up in anhydrous $CDCl_3$. To a 0.5 mL aliquot of this solution was added 0.4 mL of a 20 mM solution (0.8 equiv.) of Et_3PO in anhydrous $CDCl_3$.The mixture was then transferred to an NMR tube. Separately, a capillary tube which was closed at one end, was filled with the 20 mM solution of Et_3PO in $CDCl_3$, before being sealed with Teflon tape and inserted into the NMR tube containing the compound/Et_3PO mixture. The NMR tube was sealed and the ^{31}P{^{1}H} NMR spectrum was recorded, from which the AN for each compound was calculated using the equation; $AN = 2.21\ (\delta_{sample} - 41.0)$.

DFT calculations

These calculations were undertaken using the ORCA 4.2.1 computational software.[45] Optimizations and analytical frequency calculations were performed at the RI-B97-D3/def2-SVP level of theory[46–48] and single-point energies and solvation corrections calculated at RIJCOSX-ωB97M-D3BJ/def2-TZVPP.[48–50] Solvation correction was implemented with the CPCM model[51] with a dielectric constant value of 14 to represent the epoxide solvent environment. Analytical frequencies were calculated for inclusion of the Zero Point Energy (ZPE) correction and entropic contributions to the free energy term (ΔG_{298K}), as well as confirming all intermediates were true with no imaginary modes and all transition states had the correct critical frequency of decomposition (imaginary mode). All thermodynamic parameters were calculated in the standard state (298.15 K and 1 atm). Numerical precision integration grids were increase beyond the default settings, to *Grid4* for the SCF step *Grid5* for the final energy evaluation. Concentration correction for the individual species was applied as a free energy correction based on $RT\ ln(c_i/c_{atm})$[52] where c_i is the experimental concentration of the relevant species. This is particularly important in systems such as this, given the dual role of the epoxide, as both reagent and solvent.

AIMD simulations

These simulations were performed with ORCA 4.2.1 Molecular Dynamics Module, utilizing the GFN2-xtb semiempirical tight-binding quantum chemical method.[40] The simulations use the CPCM continuum solvent model during the runs. Two 50,000 step (25 ps) runs where preformed on each complex, firstly to equilibrate the structure, and then using the velocities from the equilibrium run, a production run for analysis was performed. All simulations were

performed at 298 K with a Berendsen thermostat. Graphical visualization using VMD[53] for analysis of the molecular dynamics' simulations.

QTAIM analysis

This analysis was performed using the Multiwfn software package.[54] Graphical visualization using Avogadro 1.2.0[55] program for the DFT calculations and molecular orbitals.

Computational Lewis Acidity Studies

Fluoride Ion Affinity (FIA) calculations were performed using the TMS-anchored isodesmic reaction scheme, originally proposed by Krossing[56] and recently updated by Greb.[35] All structures were optimised with B97-D3/def2-svp.[46–48] Thermal and Zero-Point energy corrections were calculated at the same level of theory. Further electronic energy calculations were performed with PW6B95-D3BJ/def2-qzvpp,[57] highlighted by Greb as the best performing DFT method.[35] Absolute FIA energies were calculated by subtracting the fluoride ion dissociation enthalpy ($\Delta H_{CCSD(T)/CBS} = 925.5\ kJ\,mol^{-1}$) from the calculated reaction enthalpies. The reaction schemes explored, for all catalytic systems, in this study were [Eqs. (1–3)]:

Non-ligated:

$$\text{catalyst} + Me_3SiF \rightarrow \text{Catalyst-}F^- + Me_3Si^+ \quad (1)$$

Ligand substitution:

$$\text{catalyst.ligand} + Me_3SiF \rightarrow \text{catalyst-}F^- + Me_3Si^+ + \text{ligand} \quad (2)$$

Isodesmic ligated:

$$\text{catalyst.ligand} + Me_3SiF \rightarrow \text{catalyst} \cdot \text{ligand-}F^- + Me_3Si^+ + \text{ligand} \quad (3)$$

In the above reaction schemes ligand refers to THF or EtOH for the respective catalytic systems.

^{31}P-NMR calculations were performed using TPSSh-D3BJ/pcSeg-2[58,59] and associated auxiliary basis sets, on the B97-D3/def2-svp optimised geometries. Integration grids were further increased to *Grid5* and *FinalGrid6* to ensure smooth and accurate energy evaluations. This combination of functional and basis sets has been shown to perform well for NMR chemical shift calculations.[60] Solvation effects (in chloroform) on the chemical shifts were accounted for using the CPCM method.[51] Calculated Acceptor Numbers (CAN) were calculated using $CAN = 2.21 \times (\delta_{OPMe3} - \delta_{adduct})$, where $OPMe_3$ was used rather than $OPEt_3$. QTAIM calculations, using Multiwfn, for analysis of the phosphorus to oxygen *lcp* were performed on the TPSSh-D3BJ wavefunction.[54]

Acknowledgements

A.H. would like to thank the Department of Biosciences and Chemistry and the Biomolecular Sciences Research Centre (BMRC) at Sheffield Hallam University for funding. C.W. and L.A.M. would like to thank both the Universidad de Alcalá and the Comunidad de Madrid for funding (Programa de Atracción de Talento 2019: Modalidad 1; Award number 2019-T1/AMB-13037). J.D.B thanks the Universidad de Alcalá for a Predoctoral Fellowship. We also thank Prof. Daniel Miguel (Universidad de Valladolid) for help in measuring and refining the X-ray crystal structures of ***GaL^{Me}.THF*** *and* ***GaL^{Cl}.H$_2$O****. We would like to also acknowledge funding from the Spanish Government (RTI2018-094840-BC31) and Universidad de Alcalá (UAH-AE-2017-2).*

Conflict of Interest

The authors declare no conflict of interest.

Keywords: gallium · aminotrisphenolate ligands · carbon dioxide · cyclic carbonates · DFT study.

[1] For examples, see: a) Q. Liu, L. Wu, R. Jackstell, M. Beller, *Nat. Commun.* **2015**, *6*, 5933; b) Y. Zhang, T. Zhang, S. Das, *Green Chem.* **2020**, *22*, 1800–1820; c) T. Fujihara, Y. Tsuji, *Front. Chem.* **2019**, *7*, 430; d) Y. Yang, J.-W. Lee, *Chem. Sci.* **2019**, *10*, 3905–3926; e) W. Schilling, S. Das, *ChemSusChem.* **2020**, *13*, 6246–6258; f) X. Jiang, X. Nie, X. Guo, C. Song, J. G. Chen, *Chem. Rev.* **2020**, *120*, 7984–8034; g) A. Liu, M. Gao, X. Ren, F. Meng, Y. Yang, L. Gao, Q. Yang, T. Ma, *J. Mater. Chem. A.* **2020**, *8*, 3541–3562.

[2] M. Morita, M. Ishikawa, Y. Matsuda, in *Lithium Ion Batteries: Fundamentals and Performance* (Eds.: M. Wakihara, O. Yamamoto), Wiley, **1998**, pp. 156–180.

[3] For examples, see: a) G. L. Gregory, L. M. Jenisch, B. Charles, G. Kociok-Köhn, A. Buchard, *Macromolecules* **2016**, *49*, 7165–7169; b) F. Siragusa, E. Van Den Broeck, C. Ocando, A. J. Müller, G. De Smet, B. U. W. Maes, J. De Winter, V. Van Speybroeck, B. Grignard, C. Detrembleur, *ACS Sustainable Chem. Eng.* **2021**, *9*, 1714–1728; c) W. Yu, E. Maynard, V. Chiaradia, M. C. Arno, A. P. Dove, *Chem. Rev.* **2021**, DOI: 10.1021/acs.chemrev.0c00883.

[4] For an overview, see: a) L. Maisonnueve, O. Lamarzelle, E. Rix, E. Grau, H. Cramail, *Chem. Rev.* **2015**, *115*, 12407–12439; b) C. Carré, Y. Ecochard, S. Caillol, L. Avérous, *ChemSusChem.* **2019**, *12*, 3410–3430; c) H. Blattmann, M. Fleischer, M. Bähr, R. Mülhaupt, *Macromol. Rapid Commun.* **2014**, *35*, 1238–1254.

[5] For selected examples, see: a) A. Duval, L. Avérous, *ACS Sustainable Chem. Eng.* **2017**, *5*, 7334–7343; b) V. Laserna, G. Fiorani, C. J. Whiteoak, E. Martin, E. Escudero-Adán, A. W. Kleij, *Angew. Chem. Int. Ed.* **2014**, *53*, 10416–10419; *Angew. Chem.* **2014**, *126*, 10584–10587; c) A. Khan, L. Yang, J. Xu, L. Y. Jin, Y. J. Zhang, *Angew. Chem. Int. Ed.* **2014**, *53*, 11257–11260; *Angew. Chem.* **2014**, *126*, 11439–11442; d) W. Guo, J. E. Gómez, À. Cristòfol, J. Xie, A. W. Kleij, *Angew. Chem. Int. Ed.* **2018**, *57*, 13735–13747; *Angew. Chem.* **2018**, *130*, 13928–13941; e) H. Wang, M. M. Lorion, L. Ackermann, *ACS Catal.* **2017**, *7*, 3430–3433.

[6] A. A. Marciniak, K. J. Lamb, L. P. Ozorio, C. J. A. Mota, M. North, *Curr. Opin. Green Sustain. Chem.* **2020**, *26*, 100365.

[7] a) A. J. Kamphuis, F. Picchioni, P. P. Pescarmona, *Green Chem.* **2019**, *21*, 406–448; b) H. Büttner, L. Longwitz, J. Steinbauer, C. Wulf, T. Werner, *Top. Curr. Chem.* **2017**, *375*, 50; c) M. Alves, B. Grignard, R. Mereau, C. Jerome, T. Tassaing, C. Detrembleur, *Catal. Sci. Technol.* **2017**, *7*, 2651–2684; d) C. Martín, G. Fiorani, A. W. Kleij, *ACS Catal.* **2015**, *5*, 1353–1370; e) J. W. Comerford, I. D. V. Ingram, M. North, X. Wu, *Green Chem.* **2015**, *17*, 1966–1987.

[8] M. North, R. Pasquale, *Angew. Chem. Int. Ed.* **2009**, *48*, 2946–2948; *Angew. Chem.* **2009**, *121*, 2990–2992.

[9] For references relating to the catalysts in Scheme 1b, see: a) W. Clegg, R. W. Harrington, M. North, R. Pasquale, *Chem. Eur. J.* **2010**, *16*, 6828–6843; b) C. J. Whiteoak, N. Kielland, V. Laserna, E. Escudero-Adán, E. Martin, A. W. Kleij, *J. Am. Chem. Soc.* **2013**, *135*, 1228–1231; c) Y. Qin, H. Guo, X. Sheng, X. Wang, F. Wang, *Green Chem.* **2015**, *17*, 2853–2858; For a relative benchmarking study of these three selected catalysts, see:d) J. Rintjema, A. W. Kleij, *ChemSusChem.* **2017**, *10*, 1274–1282.

[10] a) K. A. Andrea, F. M. Kerton, *ACS Catal.* **2019**, *9*, 1799–1809; b) Z. Chen, J.-L. Yang, X.-Y. Lu, L.-F. Hu, X.-H. Cao, G.-P. Wu, X.-H. Zhang, *Polym. Chem.* **2019**, *10*, 3621–3628; c) C.-J. Zhang, S.-Q. Wu, S. Boopathi, X.-H.

Zhang, X. Hong, Y. Gnanou, X.-S. Feng, *ACS Sustainable Chem. Eng.* **2020**, *8*, 13056–13063.
[11] Simple aryl boronic acids have also been applied as catalysts, however, their mode of catalytic action was found to be through hydrogen-bonding interactions and not directly with the boron atom, see: J. Wang, Y. Zhang, *ACS Catal.* **2016**, *6*, 4871–4876.
[12] I. Shibata, I. Mitani, A. Imakuni, A. Baba, *Tetrahedron Lett.* **2011**, *52*, 721–723.
[13] H. A. Baalbaki, H. Roshandel, J. E. Hein, P. Mehrkhodavandi, *Catal. Sci. Technol.* **2021**, *11*, 2119–2129.
[14] Indium Organic Frameworks (IOFs) have also been applied as catalysts, see: a) S.-L. Hou, J. Dong, Z.-H. Jiao, X.-L. Jiang, X.-P. Yang, B. Zhao, *Inorg. Chem. Front.* **2018**, *5*, 1694–1699; b) Y. Yuan, J. Li, X. Sun, G. Li, Y. Liu, G. Verma, S. Ma, *Chem. Mater.* **2019**, *31*, 1084–1091.
[15] In Ref. [13], examples of GaX_3 (X = Br and I) can be found exhibiting catalytic activity in the screening process, but full optimization with these compounds has not been reported.
[16] a) G. K. S. Prakash, T. Matthew, G. A. Olah, *Acc. Chem. Res.* **2012**, *45*, 565–577; b) S. Dagorne, R. Wehmschulte, *ChemCatChem.* **2018**, *10*, 2509–2520.
[17] a) S. Dagorne, M. Normand, E. Kirillov, J.-F. Carpentier, *Coord. Chem. Rev.* **2013**, *257*, 1869–1886; b) A. C. Deacy, C. B. Durra, C. K. Williams, *Dalton Trans.* **2020**, *49*, 223–231.
[18] For an overview, see: a) D. Y. Bae, Y. Kim, J. Cha, E. Lee, *Coord. Chem. Rev.* **2020**, *419*, 213402; b) G. Licini, M. Mba, C. Zonta, *Dalton Trans.* **2009**, 5265–5277.
[19] C. J. Whiteoak, E. Martin, M. Martínez Belmonte, J. Benet-Buchholz, A. W. Kleij, *Adv. Synth. Catal.* **2012**, *354*, 469–476.
[20] C. Miceli, J. Rintjema, E. Martin, E. C. Escudero-Adán, C. Zonta, G. Licini, A. W. Kleij, *ACS Catal.* **2017**, *7*, 2367–2373.
[21] R. J. Motekaitis, A. E. Martell, S. A. Koch, J. W. Hwang, D. A. Quarless Jr., M. J. Welch, *Inorg. Chem.* **1998**, *37*, 5902–5911.
[22] R. S. Ghadwal, A. Singh, *Indian J. Chem.* **2007**, *46 A*, 768–771.
[23] C. J. Whiteoak, N. Kielland, V. Laserna, F. Castro-Gómez, E. Martin, E. C. Escudero-Adán, C. Bo, A. W. Kleij, *Chem. Eur. J.* **2014**, *20*, 2264–2275.
[24] F. Della Monica, A. Buonerba, A. Grassi, C. Capacchione, S. Milione, *ChemSusChem.* **2016**, *9*, 3457–3464.
[25] D. J. Darensbourg, D. R. Billodeaux, *C. R. Chim.* **2004**, *7*, 755–761.
[26] See for an example: M. Fleischer, H. Blattmann, R. Mülhaupt, *Green Chem.* **2013**, *15*, 934–942.
[27] C. J. Whiteoak, E. Martin, E. Escudero-Adán, A. W. Kleij, *Adv. Synth. Catal.* **2013**, *355*, 2233–2239.
[28] For an overview of backbiting to generate cis- and trans- cyclic carbonates, see: D. J. Darensbourg, *Polym. Degrad. Stab.* **2018**, *149*, 45–51.
[29] Y. Hu, J. Steinbauer, V. Stefanow, A. Spannenberg, T. Werner, *ACS Sustainable Chem. Eng.* **2019**, *7*, 13257–13269.
[30] To the best of our knowledge there are no reports of the di-cyclic carbonate product derived from dicyclopentadiene di-epoxide (**24a**).
[31] For an example of the synthesis and use of **7a-[D$_8$]**, see: W. Liu, W. Li, A. Spannenberg, K. Junge, *Nat. Catal.* **2019**, *2*, 523–528.
[32] Cyclic carbonates can be readily converted to polycarbonates, see Ref. [3].
[33] For examples of the application of fully deuterated propylene carbonate, see: a) T. Yamaguchi, K. Yoshida, T. Yamaguchi, Y. Kameda, K. Ikeda, T. Otomo, *J. Phys. Chem. B* **2017**, *121*, 5355–5362; b) Y. M. Delavoux, M. Gilmore, M. P. Atkins, M. Swadzba-Kwasny, J. D. Holbrey, *Phys. Chem. Chem. Phys.* **2017**, *19*, 2867–2876; c) K. W. Schroder, A. G. Dylla, L. D. C. Bishop, E. R. Kamilar, J. Saunders, L. J. Webb, K. J. Stevenson, *J. Phys. Chem. Lett.* **2015**, *6*, 2888–2891; d) F. Qi, R. Boehmer, H. Sillescu, *Phys. Chem. Chem. Phys.* **2001**, *3*, 4022–4028.
[34] a) U. Mayer, V. Gutmann, W. Gerger, *Monatsh. Chem.* **1975**, *106*, 1235–1257; b) M. A. Beckett, G. C. Strickland, J. R. Holland, K. S. Varma, *Polymer* **1996**, *37*, 4629–4631.
[35] P. Erdmann, J. Leitner, J. Schwarz, L. Greb, *ChemPhysChem.* **2020**, *21*, 987–994.
[36] For selected examples see: a) Ref. [23]; b) V. Butera, H. Detz, *ACS Omega* **2020**, *5*, 18064–18072; c) F. D. Bobbink, D. Vasilyev, M. Hulla, S. Chamam, F. Menoud, G. Laurenczy, S. Katsyuba, P. J. Dyson, *ACS Catal.* **2018**, *8*, 2589–2594; d) Y. Wu, X. Song, J. Zhang, S. Xu, L. Gao, J. Zhang, G. Xiao, *Chem. Eng. Sci.* **2019**, *201*, 288–297; e) N. Liu, Y.-F. Xie, C. Wang, S.-J. Li, D. Wei, M. Li, B. Dai, *ACS Catal.* **2018**, *8*, 9945–9957; f) M. Alves, R. Méreau, B. Grignard, C. Detrembleur, C. Jérôme, T. Tassaing, *RSC Adv.* **2017**, *7*, 18993–19001; g) J. A. Castro-Osma, M. North, W. K. Offermans, W. Leitner, T. E. Müller, *ChemSusChem.* **2016**, *9*, 791–794; h) F. Castro-Gómez, G. Salassa, A. W. Kleij, C. Bo, *Chem. Eur. J.* **2013**, *19*, 6289–6298.
[37] J. González-Fabra, F. Castro-Gómez, W. M. C. Sameera, G. Nyman, A. W. Kleij, C. Bo, *Catal. Sci. Technol.* **2019**, *9*, 5433–5440.
[38] H. Plommer, L. Stein, J. N. Murphy, N. Ikpo, N. Mora-Diez, F. M. Kerton, *Dalton Trans.* **2020**, *49*, 6884–6895.
[39] C. Bannwarth, E. Caldeweyher, S. Ehlert, A. Hansen, P. Pracht, J. Seibert, S. Spicher, S. Grimme, *WIREs Comput. Mol. Sci.* **2021**, *11*, e1493.
[40] C. Bannwarth, S. Ehlert, S. Grimme, *J. Chem. Theory Comput.* **2019**, *15*, 1652–1671.
[41] S. Grimme, *J. Chem. Theory Comput.* **2019**, *15*, 2847–2862.
[42] E. Espinosa, E. Molins, C. Lecomte, *Chem. Phys. Lett.* **1998**, *285*, 170–173.
[43] P.-W. Huang, C.-Z. Wang, Q.-Y. Wu, J.-H. Lan, G. Song, Z.-F. Chai, W.-Q. Shu, *Phys. Chem. Chem. Phys.* **2018**, *20*, 1030–1038.
[44] V. Laserna, E. Martin, E. C. Escudero-Adán, A. W. Kleij, *ACS Catal.* **2017**, *7*, 5478–5482.
[45] F. Neese, *WIREs Comput. Mol. Sci.* **2017**, *8*, e1327.
[46] F. Neese, *J. Comb. Chem.* **2003**, *24*, 1740–1747.
[47] S. Grimme, S. Ehrlich, L. Goerigk, *J. Comb. Chem.* **2011**, *32*, 1456–1465.
[48] a) F. Weigend, R. Ahlrichs, *Phys. Chem. Chem. Phys.* **2005**, *7*, 3297–3305; b) A. Schäfer, H. Horn, R. Ahlrichs, *J. Chem. Phys.* **1992**, *97*, 2571.
[49] F. Neese, F. Wennmohs, A. Henson, U. Becker, *Chem. Phys.* **2009**, *356*, 98–109.
[50] N. Mardirossian, M. Head-Gordon, *J. Chem. Phys.* **2016**, *144*, 214110.
[51] Y. Takano, K. N. Houk, *J. Chem. Theory Comput.* **2005**, *1*, 70–77.
[52] J. N. Harvey, F. Himo, F. Maseras, L. Perrin, *ACS Catal.* **2019**, *9*, 6803–6813.
[53] W. Humphrey, A. Dalke, K. Schulten, *J. Mol. Graphics* **1996**, *14*, 33–38.
[54] T. Lu, F. Chen, *J. Comput. Chem.* **2012**, *33*, 580–592.
[55] M. D. Hanwell, D. E. Curtis, D. C. Lonie, T. Vandermeersch, E. Zurek, G. R. Hutchison, *J. Cheminf.* **2012**, *4*, 17.
[56] H. Böhrer, N. Trapp, D. Himmel, M. Schleep, I. Krossing, *Dalton Trans.* **2015**, 44, 7489–7499.
[57] Y. Zhao, D. G. Truhlar, *J. Phys. Chem. A* **2005**, *109*, 5656–5667.
[58] V. N. Staroverova, G. E. Scuseria, J. Tao, J. P. Perdew, *J. Chem. Phys.* **2003**, *119*, 12129–12137.
[59] F. Jensen, *J. Chem. Theory Comput.* **2015**, *11*, 132–138.
[60] G. L. Stoychev, A. A. Auer, F. Neese, *J. Chem. Theory Comput.* **2018**, *14*, 4756–4771.

Manuscript received: June 22, 2021
Revised manuscript received: August 1, 2021
Accepted manuscript online: August 3, 2021
Version of record online: ■■, ■■■

FULL PAPERS

Computational study: A highly active catalyst system based on gallium has been developed for the conversion of CO_2 and epoxides to cyclic carbonates. The catalyst displays wide substrate scope and is operative at both ambient and elevated temperatures. DFT and Ab-Initio Molecular Dynamic studies compliment the experimental work and provide key information as to why the gallium compounds are more active than their aluminium congeners.

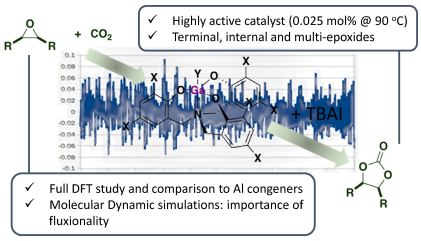

Dr. L. Álvarez-Miguel, J. D. Burgoa, Dr. M. E. G. Mosquera, Dr. A. Hamilton*, Dr. C. J. Whiteoak**

1 – 13

Catalytic Formation of Cyclic Carbonates using Gallium Aminotrisphenolate Compounds and Comparison to their Aluminium Congeners: A Combined Experimental and Computational Study